

Document Version

Preprint version Citation for published version (APA):

Alberto Sánchez-Bonaste, Luis F.S. Merchante, Carlos González-Bravo, Alberto Carnicero. (2023). Systematic measuring cortical thickness in tibiae for bio-mechanical analysis, *Computers in Biology and Medicine*, v. 163, 107123, DOI:

<https://doi.org/10.1016/j.combiomed.2023.107123>

Citing this paper

Please note that where the full-text provided on Comillas' Research Portal is the Author Accepted Manuscript or Post-Print version this may differ from the final Published version. If citing, it is advised that you check and use the publisher's definitive version for pagination, volume/issue, and date of publication details. And where the final published version is provided on the Research Portal, if citing you are again advised to check the publisher's website for any subsequent corrections.

General rights Copyright and moral rights for the publications made accessible in the Research Portal are retained by the authors and/or other copyright owners and it is a condition of accessing publications that users recognize and abide by the legal requirements associated with these rights.

- Users may download and print one copy of any publication from the Research Portal for the purpose of private study or research.
- You may not further distribute the material or use it for any profit-making activity or commercial gain
- You may freely distribute the URL identifying the publication in the Research Portal

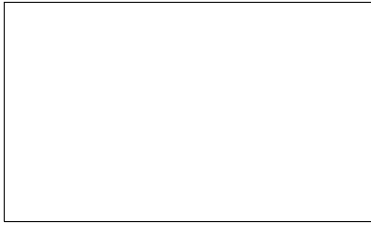
Take down policy

If you believe that this document breaches copyright please contact Comillas providing details, and we will remove access to the work immediately and investigate your claim

Graphical Abstract

Systematic measuring cortical thickness in tibiae for bio-mechanical analysis

Alberto Sánchez-Bonaste, Luis F. S. Merchante, Carlos González-Bravo, Alberto Carnicero



Highlights

Systematic measuring cortical thickness in tibiae for bio-mechanical analysis

Alberto Sánchez-Bonaste, Luis F. S. Merchante, Carlos González-Bravo, Alberto Carnicero

- Measuring algorithm that reduces human intervention to the minimum, preserving good accuracy
- Original mechanisms for aligning and orienting all bones in the same direction

Systematic measuring cortical thickness in tibiae for bio-mechanical analysis

Alberto Sánchez-Bonaste^a, Luis F. S. Merchante^b, Carlos González-Bravo^a,
Alberto Carnicero^b

*^aICAI School of Engineering. Comillas Pontifical University. Alberto Aguilera
25, 28015, Madrid, Spain*

*^bInstitute for Research in Technology. Comillas Pontifical University. Sta Cruz de
Marcenado 26, 28015, Madrid, Spain*

Abstract

Background and Objective: Measuring the thickness of cortical bone tissue helps diagnose bone diseases or monitor the progress of different treatments. This type of measurement can be performed visually from CT images by a radiologist or by semi-automatic algorithms from Hounsfield values. This article proposes a mechanism capable of measuring thickness over the entire bone surface, aligning and orienting all the images in the same direction to have comparable references and reduce human intervention to a minimum. The objective is to batch process large numbers of patients' CT images obtaining thicknesses profiles of their cortical tissue to be used in many applications.

Methods: Classical morphological and Deep Learning segmentation is used to extract the area of interest, filtering and interpolation to clean the bones and contour detection and Signed Distance Functions to measure the cortical Thickness. The alignment of the set of bones is achieved by detecting their longitudinal direction, and the orientation is performed by computing their principal component of the center of mass slice.

Results: The method processed in an unattended manner 67% of the patients in the first run and 100% in the second run. The difference in the thickness values between the values provided by the algorithm and the measures done by a radiologist was, on average, 0.25 millimetres with a standard deviation of 0.2.

Conclusions: Measuring the cortical thickness of a bone would allow us to prepare accurate traumatological surgeries or study their structural prop-

erties. Obtaining thickness profiles of an extensive set of patients opens the way for numerous studies to be carried out to find patterns between bone thickness and the patients' medical, social or demographic variables.

Keywords: Segmentation, Cortical Thickness, Thickness Measurement, Hounsfield Units

1. Introduction

Since 1972 when Godfrey Hounsfield developed the first commercial use for Computed Tomography (CT) [1] until today, this diagnostic technique has experimented a big transformation. Today it is a versatile tool that allows radiologists to get 3D images of whatever part of the body.

This experimental and noninvasive method has become a popular tool in several areas, such as direct diagnostics, surgery planning or follow-up studies, among others. In particular, the use of CAT (Computerized Axial Tomography) to characterize the tisular/organ level [2] is now considered a standard procedure for measuring human body compartments [3].

CT [4] lets researchers work into specific bone areas to identify and quantify several traits and necessary parameters, whether direct clinical uses [5] or mechanical properties for latest clinical uses [6]. Regarding clinical ones, knowledge of bone mineral density (BMD) is highly relevant [7] to preventing fracture risk in patients. Another application might be, for instance, the learning of osteoporosis pathophysiology [8] or to strive our knowledge about the effectiveness of restoring surgeries [9].

On the other hand, given the current use of numeric analysis aided by Finite Element Software [10], a significant place is spotted by geometrical and mechanical properties [11, 12] of different layers in cross-sectional areas [13], cortical thickness [14, 15] or modulus of elasticity [16].

Different methods have been developed to estimate cortical thickness from CAT images. For example, in 2010, Treece et al. [17] introduced a mathematical method to compute unbiased estimations of the cortical thickness in femur bones. Museyko et al. [18] developed an accurate and robust method based on the hypothesis of uniform cortical bone density and the deconvolution of 1D profiles. Du et al. [19] used global-local thresholding of Hounsfield Units (HU) to estimate the cortical layer in femur and tibia bones. Treece et al., [20] used the Cortical Bone Mapping technique for measuring several properties (as thickness or density) of cortical and trabecular layers, and

Humbert et al. [21] set a relation between thickness and density. They validated, using micro-CT scans of a cadaver proximal femur, an estimation of the cortical thickness in CAT from the relation between thickness and density. All these proposals require high human interaction or specific-purpose software. New developments have been made using open programming languages. In this context, Jørgensen et al. [22], or Hendriksen et al. [23] developed an open-source Python framework for tomographic images and Rosa [24] opened a code to visualize DICOM-CT files using VTK library. Those codes can be used not alone for visualising bones but also for blood and pulmonary tissue. Using their own-self code allows researchers to develop tools of massive analysis with little human intervention. For instance, thanks to artificial intelligence techniques, Kim et al.[25] measure cortical thickness automatically. They train a Convolutional Neural Network (CNN) with 12800 CAT images and use it in a segmentation process. CNNs are popular in the automatic segmentation of CAT images and are used by a lot of researchers ([26],[27],[28] or [29] among many). Recently Deng et al. [30] used them to extract the periosteal and endosteal contours of the proximal femur to differentiate cortical from the trabecular bone. Therefore, the current use of deep learning and free code languages to process DICOM-CT images has turned out to be very adaptable and helpful in identifying thresholds graphically between distinct bone layers. Training Deep Learning models suffer from two main drawbacks. The first one is the enormous amount of labelled data required for proper model training. The second is the hardware needed to train in a reasonable time, based on the expensive and recently scarce GPUs (Graphics Processing Units). For instance, the model trained by Kim et al.[25] needed thousands of images from 25 subjects segmented manually by radiologists. In addition, the models trained with images from a particular region only apply to that region. The approach developed in this paper provides a combination of different techniques proposed in the state of the art (see section 2) with some original processing that allows batch computation of cortical thickness in long bones with minimal human intervention. Segmentation and cortical thickness are evaluated with computational inexpensive techniques that result in sufficiently accurate thickness results, mainly when there is no labelled dataset to train Neural Network algorithms.

2. Materials and Methods

The mechanism described in this section automates the thickness measuring in a database of CAT images from tibiae. This approach minimizes human intervention and reduces the number of hyper-parameters. Like most techniques involving image processing, this algorithm has a heuristic behaviour that might result in a percentage of patients requiring manual adjustment. However, the proposed algorithm should succeed in most of them, simplifying data analysis tasks in large patients datasets. Figure 1 sketches the process. A reference patient dataset is chosen as the orientation and aligning reference. The remaining datasets will be processed to match those references and provide equivalent thickness measurements.

The next subsections cover the steps from the file reading to the thickness representations.

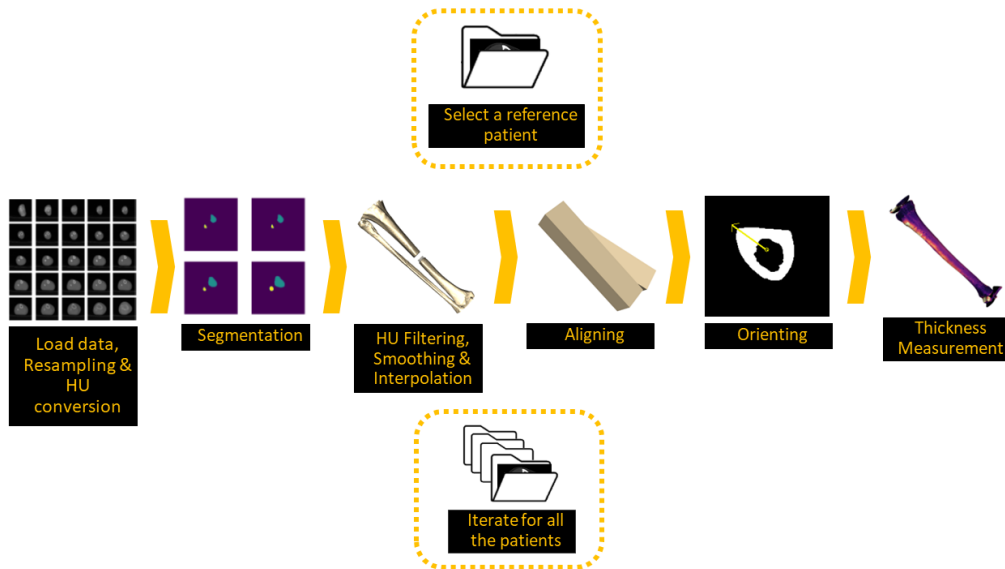


Figure 1: Diagram of the process

2.1. Reading DICOM and Computing Hounsfield Units

Converting raw DICOM values into HU requires a standard linear transformation. The Intercept and the Slope can be obtained from the DICOM files metadata.

The images shown in Figure 2 display the images converted to HU units from 767 slices CAT scan and 768x768 pixels per slice. The resolution of this scan is 0.5mm per slice and 0.255mm in both the X and Y axis. Those dimensions correspond to a tibia of approximately 383.5mm.

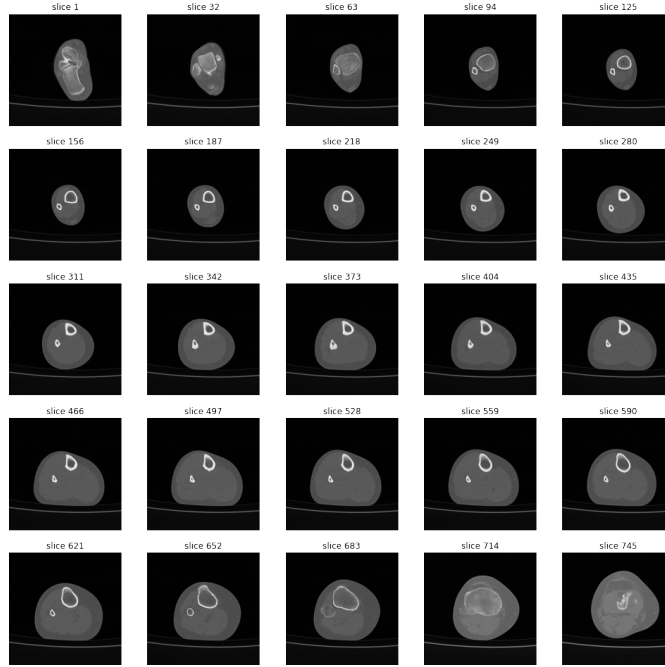


Figure 2: Tibia and fibula CAT slices

2.2. Re-sampling

The main purpose of a systematic mechanism is to automate the measuring process to a collection of CAT images from different patients. Those datasets may come from the same scanner with different parametrization or even different machines. To get comparable 3D models, the slice spacing (spacing in the Z axis) and the distance between the pixels of each slice (spacing in the X and Y axis) must be standardized. Larger spacing results in better computation times but worse resolutions. For the sample TAC image shown in Figure 2, a (1mm,1mm,1mm) re-sampling results in 384 slices of 196x196 pixels, while a (0.5mm,0.25mm,0.25m) re-sampling preserves the original size of 767 slices of 768x768 pixels. Figure 3 shows the difference in resolution between a (0.5,0.25,0.25) spacing and a (1,1,1) spacing before any processing.



(a) Sampled to (1mm,1mm,1mm) spacing (b) Sampled to (0.5mm,0.25mm,0.25mm) spacing

Figure 3: Comparison between sampling

2.3. Segmentation

Segmentation allows separating the organs and removing additional elements that are not the object of the study (a stretcher, a splint, a cast,...). Computationally, automated segmentation can be accomplished using morphological operators or neural networks. Recent advances in Neural Networks have proven their effectiveness in segmentation ([31], [32], [33], [34], [35], [36], [37]), particularly UNets ([38],[39],[40], [41],). The main drawback is the need for a huge training set to teach the network to separate a particular organ. The lack of sufficient data on labelled tibiae posed an insurmountable problem for training one of these networks. A custom UNet was trained using a labelled human torsos data set and applied to tibiae images. This dataset was augmented by re-scaling, rotating, flipping, and blurring from the original 2598 images to the final 23382 images. Unfortunately, the results were not sufficiently accurate. Figure 4 shows the results of segmenting the tibiae dataset with this network.

Morphological operators' segmentation does not require training but is a less generalizable mechanism.

The segmentation mechanism used in this study is detailed in Algorithm 1 and is inspired by other approaches from the literature [referencias]. There is only one parameter to be set in Algorithm 1, and it is the threshold to be applied in the Bounding Box Detection. Depending on its value, it's possible to extract isolated bones or the whole leg. 5 shows the bounding box selected depending on this threshold. This segmentation also relies on morphological operations like erosion and dilation, whose kernel's size is adjusted automat-

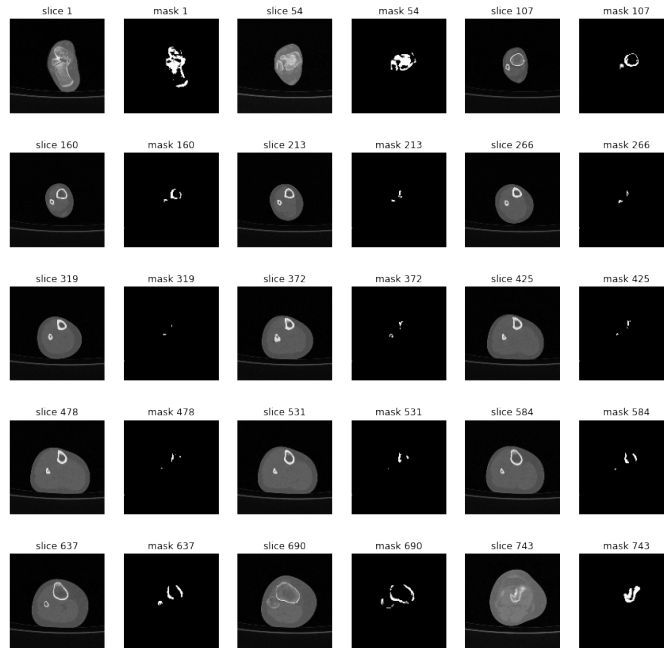


Figure 4: Torsos Trained UNet Segmentation of Tibiae

ically depending on the resolution of the images and the metadata of the DICOM files.

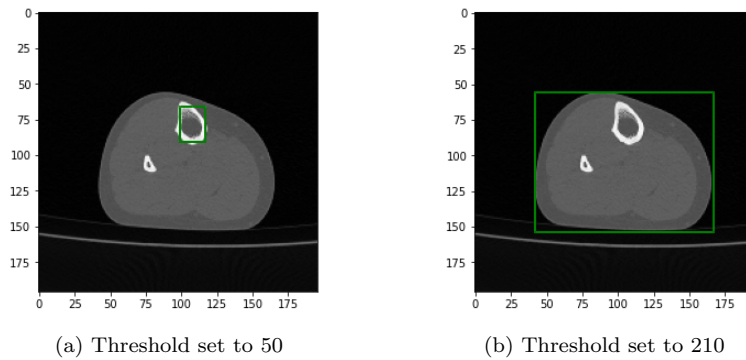


Figure 5: Effect of Thresholding Parameter in Bounding Box Selection

After the first seven steps of Algorithm 1, a first approach of the mask is generated. This mask is based on connected regions that should match the whole leg or the bones sections (tibia and fibula), depending on the purpose of

the segmentation. Those regions are labelled in step 8. This labelling allows the extraction of the tibia, the fibula or both. However, some intelligence needs to be applied because many connected regions might appear depending on the artefacts that survived the erosion operators. However, with high probability, selecting the larger regions (step 9) should allow overcoming this issue. Eventually, stronger dilation and erosion are used to fill holes on the masks (step 10 and 11) just before selecting the label of the connected region to extract (step 12).

Algorithm 1 Morphological Segmenter

- | | |
|----------------------------------|---|
| 1: Standardize values | |
| 2: Bounding Box Detection | ▷ based on a thresholded image |
| 3: KMean inside the Bounding Box | ▷ find 2 clusters |
| 4: Threshold image | ▷ based on the mean value of two centroids |
| 5: Small erosion | ▷ to remove artifacts |
| 6: Average dilation | ▷ to remove holes |
| 7: Average erosion | ▷ to restore original size |
| 8: Label connected regions | |
| 9: Keep larger regions | ▷ to avoid artifacts |
| 10: Large dilation | ▷ to remove big holes inside the bone |
| 11: Large erosion | ▷ to restore original size |
| 12: Extract Label | ▷ to extract tibia, fibula or the whole leg |
-

Figure 6 and Figure 7 show the masks computed for 25 equally distributed slices segmenting the tibia and the leg, respectively. It can be seen from those figures that segmenting larger elements is more robust than extracting isolated bones. This segmentation mechanism does not perform well on complex bone structures like the instep or the head of the tibia. The heuristic nature of this algorithm may produce empty masks that will generate gaps in the 3D model. This issue can be fixed with interpolation if the gap is not too large. Other slices have more serious problems, like the mask from slice 323 in Figure 6. This mask has created a hole inside the tibia that will be interpreted as a region with zero HU values once this mask is applied to the image. This region will be mistaken for trabecular tissue when the algorithm filter out other than cortical HU values. This is the main reason why leg segmentation is preferred to tibia segmentation. Tibia will still be able to be separated in a later step.

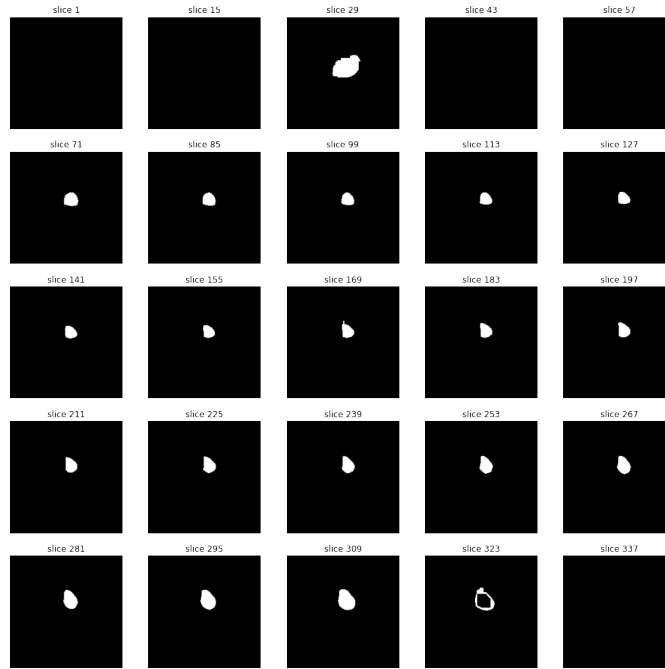


Figure 6: Tibia Segmentation

2.4. Interpolation

The heuristic behaviour of the tibial or leg segmentation may produce empty masks resulting in blank slices. If the gap is not too important, it can be fixed with two post-processing:

- Smart Bounding Box Selection. This step detects if the bounding box is too small. This is easy to generalize if the pixel spacing from DICOM metadata is known. Let's say that images are low resolution with 1mm per pixel. Knowing the size of a regular tibia, any mask slice should have an area larger than one square centimetre. That would match with a bounding box of 10x10 pixels. If the generated bounding box is smaller than this area, then the hyper-parameter of the Bounding Box selection algorithm is decreased automatically, and the algorithm is rerun until the area of the Bounding Box generated results larger than one squared centimetre. This algorithm can also be run against other resolutions without human intervention because the minimum area is easily calculated. For instance, if the images have 0.25mm per

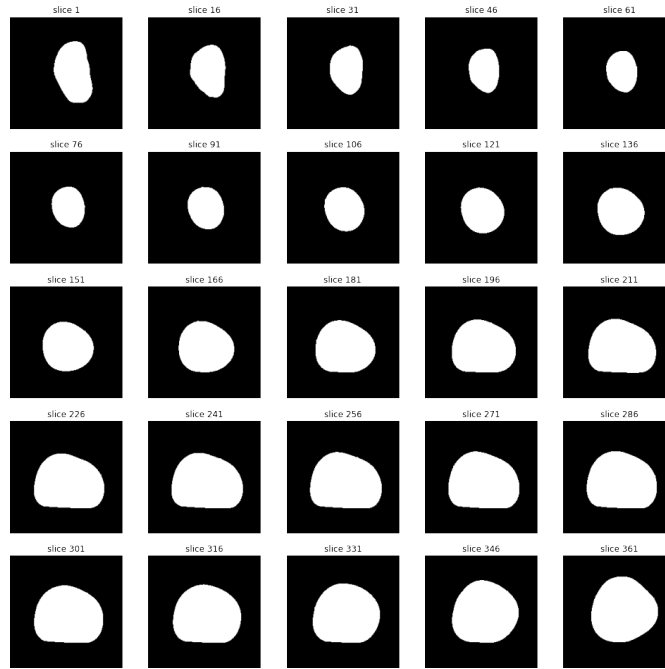


Figure 7: Leg Segmentation

pixel, the area that would match one square centimetre will be 100x100 pixels.

- Interpolation. If, after adjusting the Bounding Box to produce realistic masks, they are still missed, and if the gap is not too important, it can be regenerated through any interpolation mechanism.

Figures 8a and 8a show the difference between applying or not this two-step post-processing.

2.5. HU filtering and Smoothing

Once the mask is computed, it can be applied to the original images. The masked images are then passed through a series of filters enumerated in Algorithm 2

Figure 9a and Figure 9b show the effect of this filtering and processing.

2.6. Aligning and Orienting 3D Models

As stated before, the main purpose of a systematic mechanism is automation. CAT images are not always captured under the same conditions



(a) Without Smart Bounding Box and Interpolation (b) With Smart Bounding Box and Interpolation

Figure 8: Effect of the Smart Bounding Box Selection and Interpolation

Algorithm 2 Pre-processing of masked images

- | | |
|--|--|
| 1: HU filtering | ▷ Based on a minimum HU and a maximum HU |
| 2: Image Binarization | ▷ Selected HU are assigned value 255 and 0 otherwise |
| 3: Gaussian Smoother | |
| 4: Marching Cubes Mesh Generator | ▷ To generate the mesh |
| 5: Windowed Sinc Function Interpolation Kernel | ▷ To relax the mesh |
-

or in the same patients' positions. Even if the technician does his best to recreate the scanning condition, natural rotations of the articulations result in miss-aligned or miss-oriented tibiae.

Those problems are addressed separately.

2.6.1. *Aligning*

Aligning tibiae means aligning their axial axis in the same direction. Intuitively this means placing all the tibiae in parallel. Obtaining a representative direction of a 3D mesh is not straightforward. Some algorithms rotate objects in the three dimensions and compute different distances between the mesh's original vertex and the rotated replica's vertex. This implies tons of computations. The approach followed for aligning tibiae is a simplification that works with long bones. The idea is quite simple. The first step is to

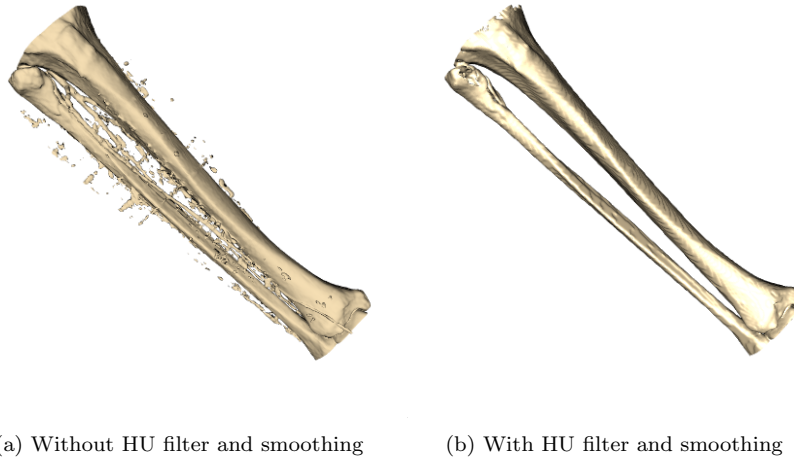


Figure 9: Effect of HU filtering and smoothing in the mesh

simplify the shape of the bones using bounding boxes (Figure 10b). The second step is to obtain the normal of one of the small sides. This normal can be used as a representative direction of each bone. The angle between the representative directions of two tibiae can be calculated and used to rotate one with respect to another. For this method to work correctly, the same side of the bounding box must be selected in both tibiae. This can be detected if the angle between the two normals is abnormally large. If this is the case, it means that the angle has been computed using opposite normals and can be fixed by changing the sign of one of the vectors. This mechanism limits the aligning capabilities of this algorithm to tibiae with less than 90 degrees between their main axes, which does not occur frequently.

Figure 10 shows the original tibiae of two patients (Figure 10a) and their bounding box simplification (Figure 10b) and the result after the correction (Figure 10c).

2.6.2. Orienting

Correcting the orientation of the tibiae means rotating them around their axial axis to get all the tibia crests pointing in the same direction. The algorithm proposed is also very simple. The centre of the mass slice is used as a reference, and a significant direction is obtained using a maximum variance projection mechanism like Principal Component Analysis (PCA). This direction is intended to represent the orientation of the tibia. If the same

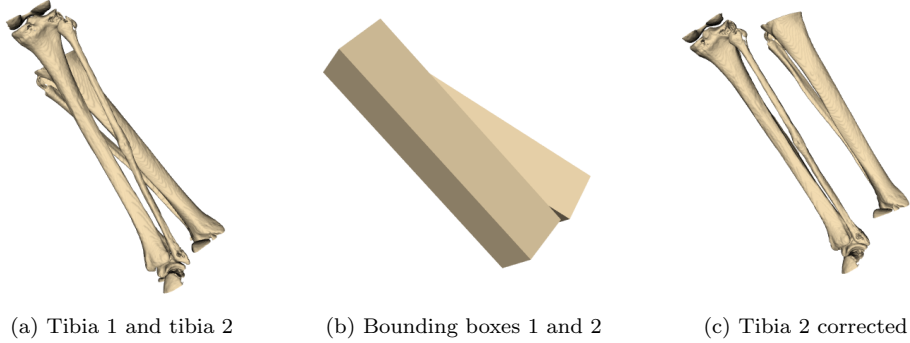


Figure 10: Aligning algorithm on Tibiae 1 and 2

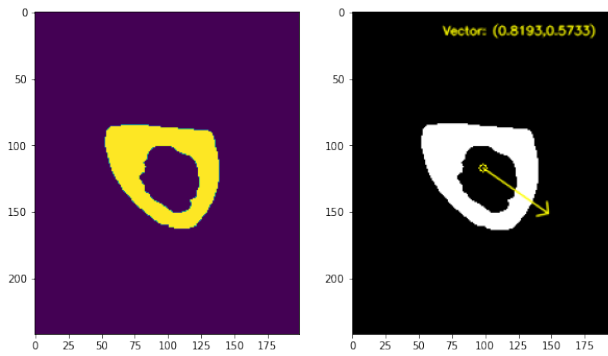
process is reproduced for all patients' tibiae, one reference direction could be defined and rotate all tibiae according to it. Figure 11 shows the representative directions for two patients' tibiae. Between the vector defined in Figure 11a and the vector defined in Figure 11b, 66.4 degrees have been measured. Figure 12 shows the effect of applying the correction to one patient's tibia.

For this method to work correctly, the maximum variance direction computed as the main eigenvector must be pointing towards the same tibia region. It might happen that PCA properly detects the main eigenvector but pointing towards the opposite direction. Figure 13 depicts this scenario. That could result in rotations larger than 90 degrees. If the tibiae are scanned equally with the patient lying upwards and belonging to the same side of the body, such rotations should not be possible. If a large rotation angle is detected, then changing the sign of the vector components should provide the right rotation angle.

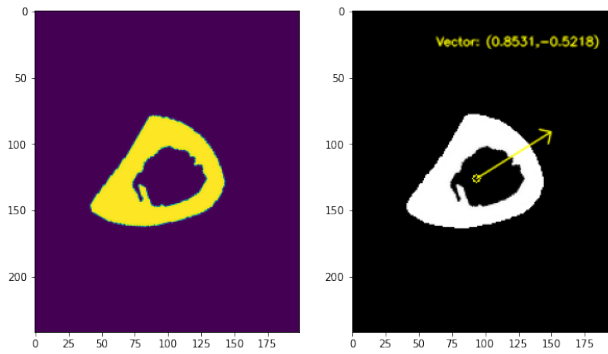
This mechanism could be applied to orient any long bones, however, its efficacy depends on the efficacy of PCA to detect the same direction. Maximum variance direction is more stable in a tibia axial section due to its less symmetrical aspect. However, an axial section of a femur is less irregular making the orientation algorithm less stable than when applied to tibiae. This can be verified in the Results section.

2.7. Measuring Cortical Thickness

Measuring cortical thickness is the key part of this paper. The algorithm relies on four steps: (i) extracting the external contour of tibiae, (ii) applying a skeletonize morphological operator to the binarized slice of the 3D model

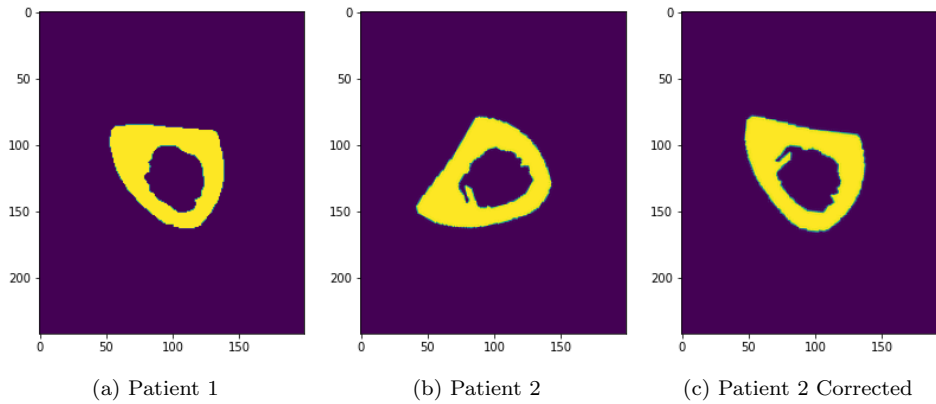


(a) Center of Mass Slice of Patient 1



(b) Center of Mass Slice of Patient 1

Figure 11: Representative Directions of Two Slices for Two Patients



(a) Patient 1

(b) Patient 2

(c) Patient 2 Corrected

Figure 12: Patient 2 Tibia Corrected to Fit Patient 1 Orientation

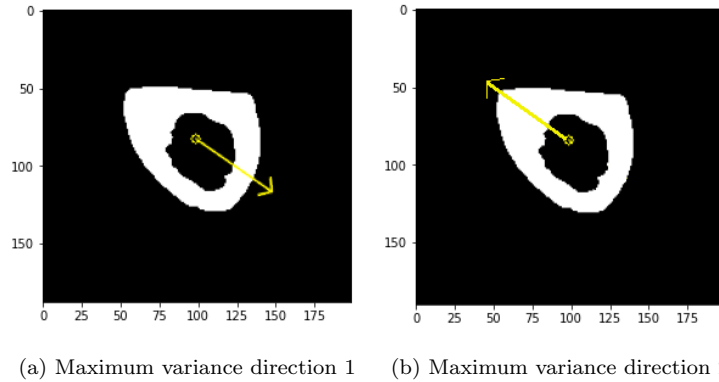


Figure 13: Two possible maximum variance directions

reducing the cortical tissue to a one-pixel representation without breaking connectivity ([42], [43]), (iii) computing the Signed Distance Function (SDF) of the external contour, and (iv) evaluating this function in the skeleton. The resulting values must be doubled because the skeleton is supposed to be the inner region of the cortical tissue. Algorithm 3 summarizes the steps, and Figure 14 shows the output image after each step. Figure 14d displays with colours the evaluation of SDF in the skeleton multiplied by two. Warmer colour means thicker cortical tissue, and colder colours mean thinner. The values of the thickness are expressed in pixels. The translation to mm is trivial, considering the sampling applied to the image. The images displayed in this document are computed at the highest resolution, that is, 0.25mm on both axis X and Y. Thus, distances measured in pixels must be divided by 4 to obtain thickness in millimetres.

Algorithm 3 Cortical Thickness Measuring Algorithm

- 1: **for each slice do**
 - 2: Generate contours
 - 3: Extract external contour \triangleright this step allows to separate bones
 - 4: Compute SDF of the external contour
 - 5: Compute skeleton
 - 6: Evaluate SDF in skeleton
 - 7: Multiply per 2
 - 8: **end for**
-

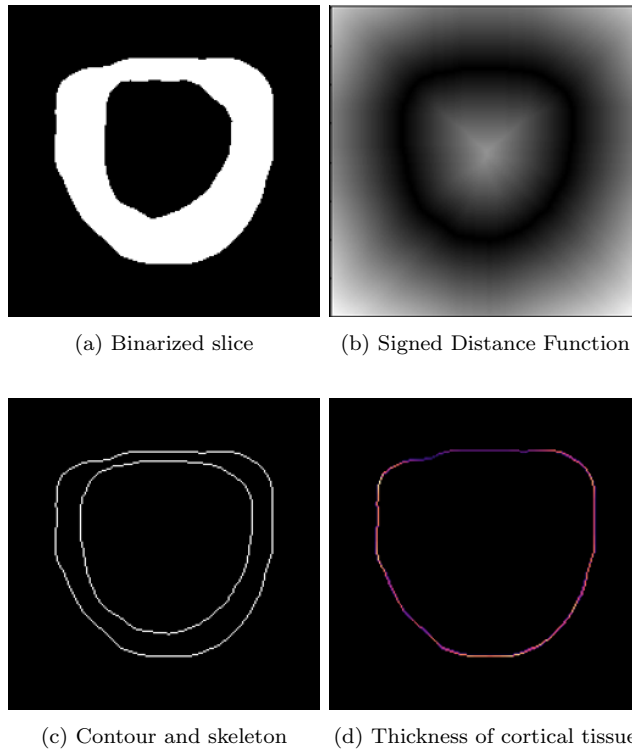


Figure 14: The average and standard deviation of critical parameters

2.8. Thickness Representations

Depending on the purpose, the thickness can be represented differently. Thickness information of a regular tibia serialized may take 200MB of data, at high resolution, the size may increase to around 2GB per tibia. This amount of data might be excessive for different applications. Recreating a 3D-printed bone requires full resolution, but training a multivariate regressor to predict the appearance of structural problems or to perform a statistical study about tibia cortical thickness requires much fewer data.

The incoming sections propose three alternatives to display the thickness values.

2.8.1. Computing Profiles

A tibia profile is a 1D representation of cortical thickness taken from a cut at a certain height. A good approximation of tibial morphology would be taking a few tens of those cuts. This consumes lower memory, and any

later processing will be considerably faster. Taking 20 cuts reduces the size of thickness information from 200MB to less than 5MB. Figure 15 shows an example of those cuts, and Figure 16 shows the associated thickness profiles. Note that the X values from all profiles in Figure 16 may differ. The X-axis represents the perimeter of the tibia slice corresponding to each profile. Depending on the diameter of the tibia at that height, the perimeter will be larger or smaller. That will result in more or fewer X values (measured in pixels).

To make this computation systematic, the initial cut will be taken in the centre of mass of the tibiae. Then, upper and lower cuts are taken equally spaced so that the same profile number matches the same areas regardless of the patient's tibia.



Figure 15: Cuts for profiling

2.8.2. Unwrapping Cortical Tissue

Another possibility to represent cortical thickness is to unroll the cortical tissue as if it were a carpet. Figure 17 shows the resulting surface. This trick of flattening a tibia allows us to apply all the theories of CNNs to detect irregularities in cortical tissues.

2.8.3. Coloring 3d Model

The last of the thickness representations is colouring the 3D model. This is probably the less practical from the point of view of data analysis, but it is

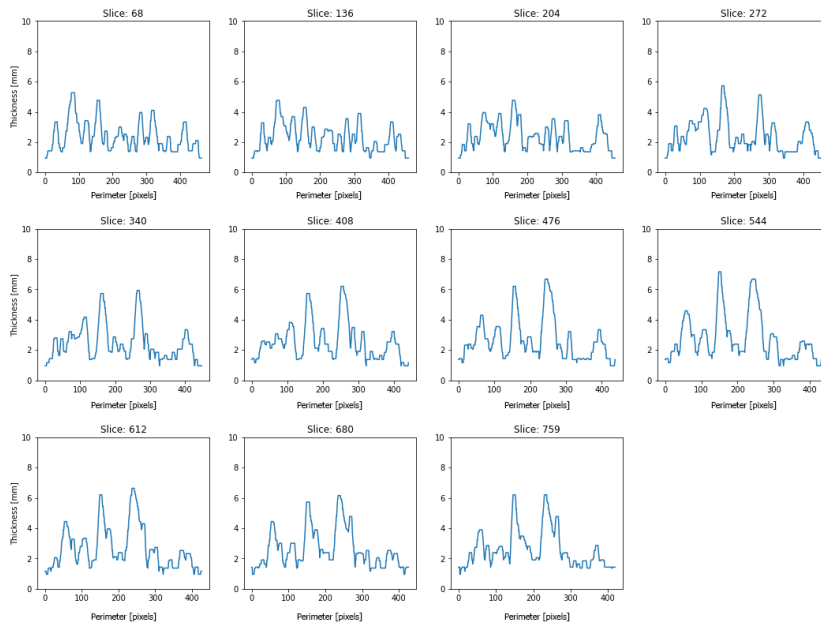


Figure 16: Profiles for the selected cuts. Thickness in millimetres

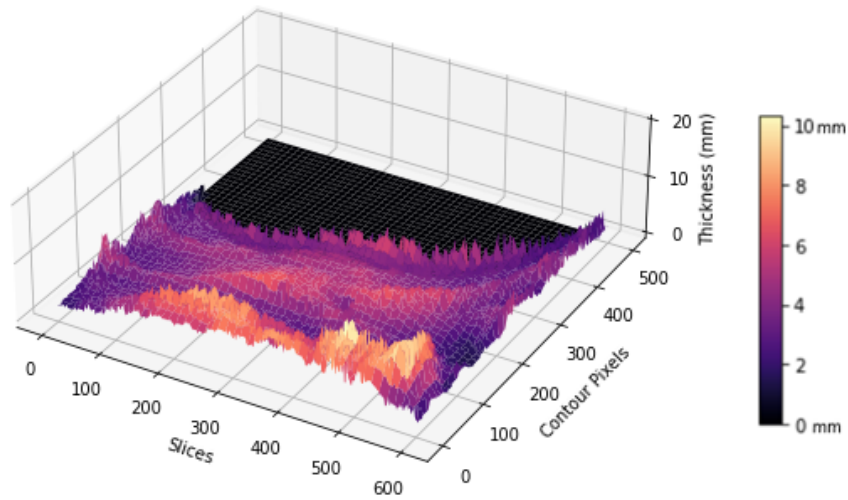


Figure 17: Unwrapped thickness surface of a tibia

the most intuitive from the human point of view. This type of visualization could assist in detecting weaknesses in the patient's tibia or prepare a surgical intervention. Figure 18 shows the 3D model coloured with the thickness

values.



Figure 18: 3D Model colored using thickness values

3. Results

The code developed in this research [44] has been tested against 15 long bones (tibiae and femora) and has successfully processed 10 out of 15 (67%) without human intervention. The 5 remaining bones required another parametrization, meaning all bones were processed in two iterations of the algorithm. Four of the five bones that required a new parametrization came from a different CAT device. Thus, accessing the scanner configuration might help to optimize the algorithm. Figure 19 shows the results after a single execution of the measuring mechanisms. The processed tibiae and femora measured in the first execution are displayed with the colours proportional to their cortical thickness. The bones that required a second run are displayed in a neutral colour showing the output of the first execution. After each run of the algorithm, the code leaves a log file where it can be easily reviewed which bones have been properly measured. These traces allow preparing a second run of the algorithm with a different parametrization to be executed only on the patient's TC that failed the first execution. As stated in the Orienting Section, Figure 19 shows worse orientation effectiveness on femorae than in tibiae for the reasons set out before.

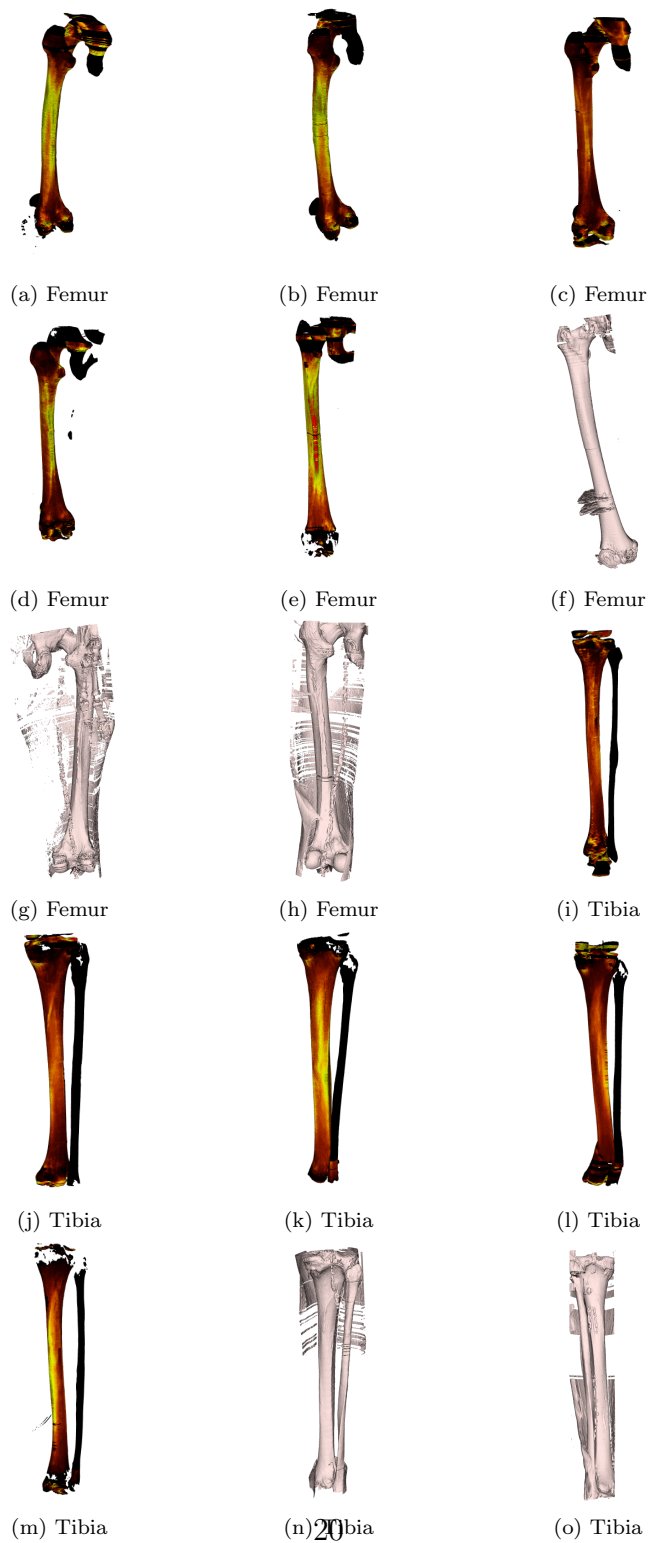


Figure 19: 3D rendered of 15 patients

To evaluate the precision of the measuring method, a slice extracted from the centre of mass of ten tibia and femora are measured manually by radiologists on the original DICOM image and automatically through the mechanism described in section 2.7. Figure 20 shows the results. Note that no aligning and orientation has been applied to the bones to evaluate the algorithm’s precision so that the radiologist can measure the thickness in the original TAC slices. Aligning and orienting it’s helpful to provide equivalent thickness profiles for different patients but does not affect the thickness measurements.

	Measure 0			Measure 1			Measure 2			Measure 3		
	Algorithm [mm]	Manual [mm]	Difference [%]	Algorithm [mm]	Manual [mm]	Difference [%]	Algorithm [mm]	Manual [mm]	Difference [%]	Algorithm [mm]	Manual [mm]	Difference [%]
leg7	12.7	12.68	0.16	4.4	4.47	-1.57	7.5	7.44	0.81	6.8	6.42	5.92
leg9	12.1	12.05	0.41	4.1	4.71	-12.95	5.3	5.48	-3.28	6.2	6.50	-4.62
leg10	13.3	12.55	5.98	4.8	5.14	-6.61	5.7	6.02	-5.32	5.9	5.78	2.08
leg9_2	3.8	4.00	-5.00	7.4	7.21	2.64	4.8	4.89	-1.84	6.8	7.26	-6.34
leg1	5.3	5.43	-2.39	3.3	3.31	-0.30	6.2	6.52	-4.91	4.8	4.59	4.58
femur7	7.6	7.95	-4.40	11.9	11.95	-0.42	12.4	11.90	4.20	9.1	9.04	0.66
femur1izq	10.2	9.38	8.74	8.6	8.64	-0.46	11.5	11.36	1.23	12.9	12.59	2.46
femur1der	9.6	9.33	2.89	11.9	12.15	-2.06	11.5	11.26	2.13	8.1	8.59	-5.70
femur9	4.8	5.14	-6.61	6.7	6.72	-0.30	11.5	11.31	1.68	5.3	5.73	-7.50
femur10	4.8	4.84	-0.83	9.0	8.99	0.11	8.4	8.74	-3.89	6.7	7.21	-7.07

Table 1: Thickness measures from Algorithm and Radiologist

Figure 21 and Table 1 show the discrepancies between the thickness measured by the radiologist and the values provided by the algorithm resulting in an average accuracy of 3.5% with a standard deviation of 2.8% (0.25 millimetres of average accuracy and 0.20 of standard deviation). Figure 21 shows a light trend to overestimate the measures than those provided by the radiologist.

4. Discussion and Conclusions

The main purpose of this project is to achieve an algorithm that allows measuring the cortical thickness in long bones to be processed in batch mode with the highest success rate possible and minimal human intervention. This information can be used for statistical analysis to find patterns between the patient’s features and their cortical thickness, to prepare surgeons for traumatological interventions, to implement an automated bone quality surveillance mechanism, or to generate artificial geometries for Finite Element Analysis and CAD systems.

We have applied classical image segmentation and thickness measurements based on filtering and morphological operators and proposed some original methods to perform batch processing of a TC database. The accuracy of the thickness measures has been evaluated against the raw Dicom images detecting underestimation of the measurements in the thicker sections of the bones. A better evaluation must be done by slicing one of these bones and measuring the actual thickness. More generalizable algorithms could be achieved using Deep Neural Networks. However, the main drawback of those algorithms is the massive amount of labelled data required for proper training. We have obtained 67% success rates on 15 patients without a Deep Learning database. More tests in larger datasets need to be performed to guarantee the success rate obtained in our study.

References

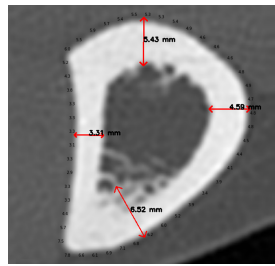
- [1] C. Richmond, Sir godfrey hounsfield, *British Medical Journal* 329 (2004) 687.
- [2] Z.-M. Wang, R. N. Pierson Jr, S. B. Heymsfield, The five-level model: a new approach to organizing body-composition research, *The American journal of clinical nutrition* 56 (1) (1992) 19–28.
- [3] S. Mattsson, B. J. Thomas, Development of methods for body composition studies, *Physics in Medicine & Biology* 51 (13) (2006) R203.
- [4] M. Mazonakis, J. Damilakis, Computed tomography: What and how does it measure?, *European journal of radiology* 85 (8) (2016) 1499–1504.
- [5] J. Baisden, V. Varghese, N. Yoganandan, 174. clinical significance of c1-c2 bone mineral density using quantitated computer tomography, *The Spine Journal* 22 (9, Supplement) (2022) S92–S93. doi:<https://doi.org/10.1016/j.spinee.2022.06.193>.
- [6] J. C. Arnone, B. D. Crist, C. V. Ward, A. S. El-Gizawy, T. Pashuck, G. J. Della Rocca, Variability of human femoral geometry and its implications on nail design, *Injury* 52 (1) (2021) 109–116.
- [7] K. Duelfer, C. Sakow, H. Chang, T. Boffeli, Assessment of bone mineral density in the distal tibia using quantitative hounsfield samples from computer tomography, *The Journal of Foot and Ankle Surgery* (2022).
- [8] L. McNamara, P. Prendergast, M. Schaffler, Bone tissue material properties are altered during osteoporosis, *Journal of Musculoskeletal and Neuronal Interactions* 5 (4) (2005) 342.
- [9] H. Liebl, T. Baum, D. C. Karampinos, J. Patsch, A. Malecki, F. Schaff, E. Eggl, E. J. Rummeny, F. Pfeiffer, J. S. Bauer, Emerging research on bone health using high-resolution ct and mri, *Current Radiology Reports* 2 (1) (2014) 1–12.
- [10] P. Henyš, M. Vořechovský, J. Stebel, M. Kuchař, P. Exner, From computed tomography to finite element space: A unified bone material mapping strategy, *Clinical Biomechanics* 97 (2022) 105704.

- [11] J.-T. Hsu, S.-P. Wang, H.-L. Huang, Y.-J. Chen, J. Wu, M.-T. Tsai, The assessment of trabecular bone parameters and cortical bone strength: a comparison of micro-ct and dental cone-beam ct, *Journal of biomechanics* 46 (15) (2013) 2611–2618.
- [12] H. Fuller, R. Fuller, R. M. R. Pereira, High resolution peripheral quantitative computed tomography for the assessment of morphological and mechanical bone parameters, *Revista brasileira de reumatologia* 55 (2015) 352–362.
- [13] R. A. Pearson, G. M. Treece, Measurement of the bone endocortical region using clinical ct, *Medical Image Analysis* 44 (2018) 28–40.
- [14] Z. S. Hostetler, J. D. Stitzel, A. A. Weaver, Comparing rib cortical thickness measurements from computed tomography (ct) and micro-ct, *Computers in biology and medicine* 111 (2019) 103330.
- [15] K. Adanty, K. N. Rabey, M. R. Doschak, K. B. Bhagavathula, J. D. Hogan, D. L. Romanyk, S. Adeeb, S. Ouellet, T. A. Plaisted, S. S. Satapathy, et al., Cortical and trabecular morphometric properties of the human calvarium, *Bone* 148 (2021) 115931.
- [16] H.-L. Huang, M.-T. Tsai, D.-J. Lin, C.-S. Chien, J.-T. Hsu, A new method to evaluate the elastic modulus of cortical bone by using a combined computed tomography and finite element approach, *Computers in biology and medicine* 40 (4) (2010) 464–468.
- [17] G. M. Treece, A. H. Gee, P. M. Mayhew, K. E. S. Poole, High resolution cortical bone thickness measurement from clinical ct data, *Med Image Anal* 14(3) (2010) 276–90.
- [18] O. Museyko, B. Gerner, K. Engelke, A new method to determine cortical bone thickness in ct images using a hybrid approach of parametric profile representation and local adaptive thresholds: Accuracy results., *PLoS One*. 12(11): e0187097 (2017). doi:10.1371/journal.pone.0187097.
- [19] W. Du, Z. J, H. J, A method to determine cortical bone thickness of human femur and tibia using clinical ct scans, in: *Proc. of the 18th International IRCOBI Conference on the Biomechanics of Injury, NordiCHI, Athens, Greece, 2018*, pp. IRC18–65.

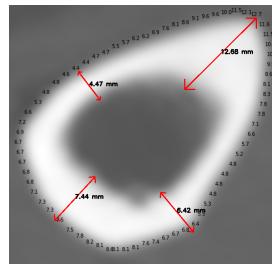
- [20] T. G., G. A., Cortical bone mapping: Measurement and statistical analysis of localised skeletal changes, *Curr Osteoporos Rep* 16(5) (2018) 617–625. doi:10.1007/s11914-018-0475-3.
- [21] L. Humbert, J. Hazrati Marangalou, L. Del Río Barquero, G. van Lenthe, van Rietbergen B., Cortical thickness and density estimation from clinical ct using a prior thickness-density relationship, *Med Phys* 43(4) (2016). doi:10.1118/1.4944501.
- [22] J. Jørgensen, E. Ametova, G. Burca, G. Fardell, E. Papoutsellis, E. Pasca, K. Thielemans, M. Turner, R. Warr, W. Lionheart, P. Withers, Core imaging library - part i: a versatile python framework for tomographic imaging, *Philos Trans A Math Phys Eng Sci* 379(2204):20200192 (2021). doi:10.1098/rsta.2020.0192.
- [23] A. Hendriksen, D. Schut, W. Palenstijn, N. Viganó, J. Kim, D. Pelt, T. van Leeuwen, K. Joost Batenburg, Tomosipo: fast, flexible, and convenient 3d tomography for complex scanning geometries in python, *Opt Express* 29(24) (2021) 40494–40513. doi:10.1364/OE.439909.
- [24] W. Rosa. Electronic references [online] (2019) [cited 10 September 2022].
- [25] Y. Kim, J. Shin, A. Lee, S. Park, S. Han, H. Hwang, Automated cortical thickness measurement of the mandibular condyle head on cbct images using a deep learning method, *Sci Rep* 11(1):14852 (2021). doi:10.1038/s41598-021-94362-7.
- [26] S. Shujaat, O. Jazil, H. Willems, A. Van Gerven, E. Shaheen, C. Politis, R. Jacobs, Automatic segmentation of the pharyngeal airway space with convolutional neural network, *J Dent* 8(111):103705 (2021). doi:10.1038/s41598-021-94362-7.
- [27] Ç. Sin, N. Akkaya, S. Aksoy, K. Orhan, U. Öz, A deep learning algorithm proposal to automatic pharyngeal airway detection and segmentation on cbct images, *Orthodontics & Craniofacial Research* 24 (2021) 117–123.
- [28] Y. Lv, J. Ke, Y. Xu, Y. Shen, J. Wang, J. Wang, Automatic segmentation of temporal bone structures from clinical conventional ct using a cnn approach, *Int J Med Robot* 17(2) (2021) e2229. doi:10.1002/rcs.2229.

- [29] X. Zhou, Automatic segmentation of multiple organs on 3d ct images by using deep learning approaches, *Adv Exp Med Biol* 1213 (2020) 135–147. doi:10.1007/978-3-030-33128-3_9.
- [30] Y. Deng, L. Wang, C. Zhao, S. Tang, X. Cheng, H. Deng, W. Zhou, A deep learning-based approach to automatic proximal femur segmentation in quantitative ct images, *Med Biol Eng Comput* 60(5) (2022) 1417–1429. doi:10.1007/s11517-022-02529-9.
- [31] K.-S. Cheng, J.-S. Lin, C.-W. Mao, The application of competitive hopfield neural network to medical image segmentation, *IEEE transactions on medical imaging* 15 (4) (1996) 560–567.
- [32] J. Chen, L. Yang, Y. Zhang, M. Alber, D. Z. Chen, Combining fully convolutional and recurrent neural networks for 3d biomedical image segmentation, *Advances in neural information processing systems* 29 (2016).
- [33] F. Milletari, N. Navab, S.-A. Ahmadi, V-net: Fully convolutional neural networks for volumetric medical image segmentation, in: 2016 fourth international conference on 3D vision (3DV), IEEE, 2016, pp. 565–571.
- [34] M. Liu, J. Dong, X. Dong, H. Yu, L. Qi, Segmentation of lung nodule in ct images based on mask r-cnn, in: 2018 9th International Conference on Awareness Science and Technology (iCAST), IEEE, 2018, pp. 1–6.
- [35] D. Jha, M. A. Riegler, D. Johansen, P. Halvorsen, H. D. Johansen, Doubleu-net: A deep convolutional neural network for medical image segmentation, in: 2020 IEEE 33rd International symposium on computer-based medical systems (CBMS), IEEE, 2020, pp. 558–564.
- [36] J.-H. Shu, F.-D. Nian, M.-H. Yu, X. Li, An improved mask r-cnn model for multiorgan segmentation, *Mathematical Problems in Engineering* 2020 (2020).
- [37] D. Müller, F. Kramer, Miscnn: a framework for medical image segmentation with convolutional neural networks and deep learning, *BMC medical imaging* 21 (1) (2021) 1–11.

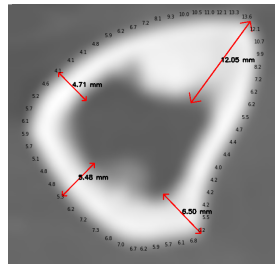
- [38] M. Z. Alom, M. Hasan, C. Yakopcic, T. M. Taha, V. K. Asari, Recurrent residual convolutional neural network based on u-net (r2u-net) for medical image segmentation, arXiv preprint arXiv:1802.06955 (2018).
- [39] Y. Weng, T. Zhou, Y. Li, X. Qiu, Nas-unet: Neural architecture search for medical image segmentation, *IEEE Access* 7 (2019) 44247–44257.
- [40] H. Huang, L. Lin, R. Tong, H. Hu, Q. Zhang, Y. Iwamoto, X. Han, Y.-W. Chen, J. Wu, Unet 3+: A full-scale connected unet for medical image segmentation, in: *ICASSP 2020-2020 IEEE International Conference on Acoustics, Speech and Signal Processing (ICASSP)*, IEEE, 2020, pp. 1055–1059.
- [41] H. Cao, Y. Wang, J. Chen, D. Jiang, X. Zhang, Q. Tian, M. Wang, Swin-unet: Unet-like pure transformer for medical image segmentation, arXiv preprint arXiv:2105.05537 (2021).
- [42] T. Y. Zhang, C. Y. Suen, A fast parallel algorithm for thinning digital patterns, *Communications of the ACM* 27 (3) (1984) 236–239.
- [43] T.-C. Lee, R. L. Kashyap, C.-N. Chu, Building skeleton models via 3-d medial surface axis thinning algorithms, *CVGIP: Graphical Models and Image Processing* 56 (6) (1994) 462–478.
- [44] A. Sanchez-Bonastre, Systematic measuring cortical thickness in tibiae for bio-mechanical analysis, <https://github.com/AlbertoSanBon/corticalMeasurement> (2022).



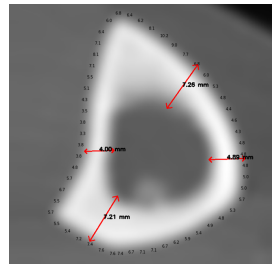
(a) Tibia 1



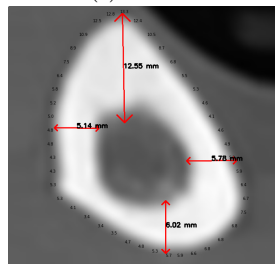
(b) Tibia 2



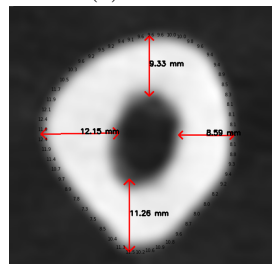
(c) Tibia 3



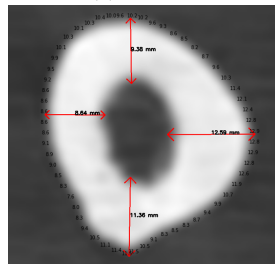
(d) Tibia 4



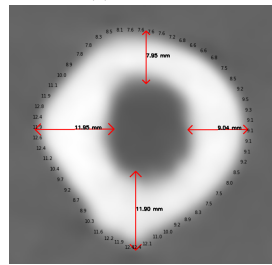
(e) Tibia 5



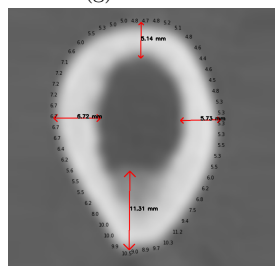
(f) Femur 1



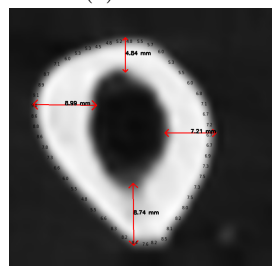
(g) Femur 2



(h) Femur 3



(i) Femur 4



(j) Femur 5

28
Figure 20: Cortical thickness at the Center of Mass in millimetres

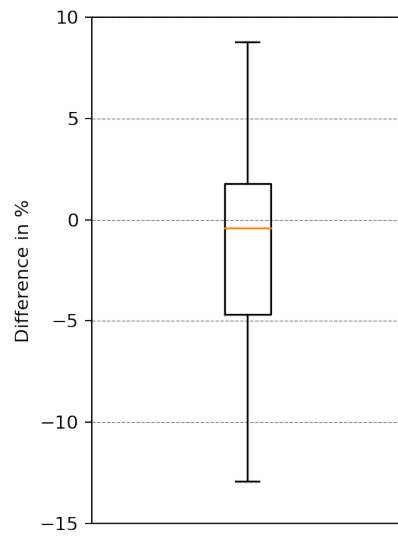


Figure 21: Distribution of discrepancies between manual and automated thickness measures